Chemical Engineering Journal 333 (2018) 572–582

Contents lists available at ScienceDirect

Chemical Engineering Journal

journal homepage: www.elsevier.com/locate/cej

Investigation of a two-dimensional model on microbial fuel cell with different biofilm porosities and external resistances

Wen-Fang Cai[a], Jia-Feng Geng[b], Kai-Bo Pu[a], Qian Ma[a], Deng-Wei Jing[b], Yun-Hai Wang[a,c,*], Qing-Yun Chen[b,c], Hong Liu[d]

[a] Department of Environmental Science and Engineering, Xi'an Jiaotong University, Xi'an 710049, China
[b] State Key Laboratory of Multiphase Flow in Power Engineering, Xi'an Jiaotong University, Xi'an 710049, China
[c] Guangdong Xi'an Jiaotong University Academy, Foshan 528000, China
[d] Department of Biological and Ecological Engineering, Oregon State University, Corvallis, OR 97331, USA

GRAPHICAL ABSTRACT

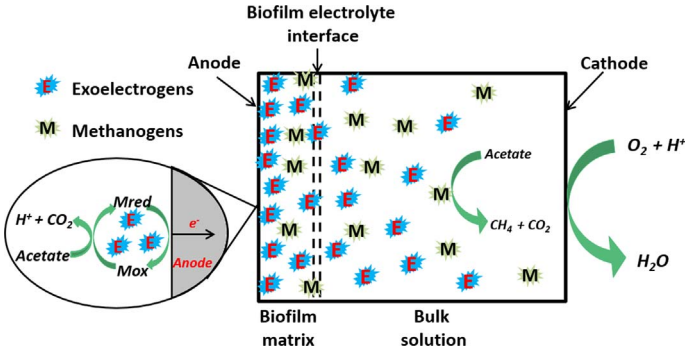

ARTICLE INFO

Keywords:
Microbial fuel cell
Mathematical model
Mass transfer
Microorganism distribution

ABSTRACT

To discuss the internal mass distribution in microbial fuel cell (MFC), a transient, two-dimensional model for single-chamber, air cathode MFC was developed in this work. This model was established by finite element method considering two kinds of microorganisms' growth, internal mass transfer and bio-electrochemical kinetics. The heterogeneous chemical components distribution in the anode chamber, the growth and spatial distribution of exoelectrogens and methanogens were discussed. The effect of biofilm porosity and external resistance on the electron transfer from redox mediator to the anode, microorganism growth and electricity generation performance in MFC was investigated. Simulation results revealed that the exoelectrogens and methanogens concentrations distributed heterogeneously with different biofilm porosities. Higher biofilm porosity was beneficial to final electron transfer step and had different impact on electricity generation at start-up and steady stage, respectively. Lower external resistances contributed to enhancing MFC performance. Our model should be helpful for the optimization of the design and operation conditions in MFCs.

1. Introduction

Microbial fuel cell (MFC) is such a bioelectrochemical device that can directly convert chemical energy of a large diversity of organic matters in domestic and industrial wastewater into electricity via catalysis of exoelectrogens. And exoelectrogens are capable of transporting

* Corresponding author at: Department of Environmental Science and Engineering, Xi'an Jiaotong University, Xi'an 710049, China.
E-mail address: wang.yunhai@mail.xjtu.edu.cn (Y.-H. Wang).

http://dx.doi.org/10.1016/j.cej.2017.09.189
Received 20 June 2017; Received in revised form 29 September 2017; Accepted 30 September 2017
Available online 01 October 2017
1385-8947/ © 2017 Elsevier B.V. All rights reserved.

electrons to a solid anode through extracellular electron transfer (EET) [1]. Nowadays, MFC has been regarded as a promising energy source of treating waste or wastewater, such as solid waste [2,3], contaminated soil/sediment [4,5], and various wastewaters [6,7] in anode chamber, and denitrification [8], heavy metals removal in cathode chamber [9,10]. Furthermore, MFC can also be used in desalination system [11], in hydrogen evolution system and in reverse electrodialysis [12,13].

However, the processes in a MFC are complex biological, physical, and electrochemical processes [14]. A number of limitations have hindered the wide implementation of MFC compared to chemical fuel cell. Specially, the output power of the MFC is several orders lower than that of chemical fuel cell. The power output is usually affected by a variety of parameters that being hard to monitor in situ, such as the population of organisms, the growth/decay rate of exoelectrogens, biofilm thickness, the substrate utilization rate inside the biofilm, the mass transfer of the reactants and products etc. These are possibly the key factors to study the electricity generation mechanism and improve the power output of a MFC. Thus, in-depth understanding of the phenomena in a MFC contributes to improving its performance. Mathematical model is a valuable tool for insight into these key components, as models can be easily modified to transform various configurations, operation conditions into simple series of mathematical expressions to detect rate-limiting steps to improve MFC's power output. Modeling has been widely used in the development of chemical fuel cells, but only a few numerical simulations have been dedicated to investigate the dimensions, operation parameters or mechanism of electron transfer in MFCs. There are three mechanisms for EET of exoelectrogens in MFC system, direct electron transfer, a solid conductive matrix and an electron shuttle [15]. Due to the uncertain electron transfer mechanism in MFC, different assumption had been made. Picioreanu et al. [16,17] developed two-dimensional and three dimensional models to simulate the growth of anodophilic and non-anodophilic populations in the biofilm and MFC performance by assuming a certain concentration of redox mediator added in the bulk solution. Picioreanu et al. [18] also developed a micro-scale individual-based two-dimensional biofilm model to evaluate the effect of initial anode pH, the bicarbonate buffer, fluid dynamics and electrode geometry on MFC performance. The model assumed the electron transfer mechanism being by soluble redox mediators, and this model opened a way to study the influence of fluid flow and any two- or three-dimensional biofilm and electrode geometry on the MFC performance. Zeng et al. [19] simulated both steady and dynamic behavior of fuel concentration, flow rate of fuel, cathodic reaction kinetics and power output on a mediator-less two-chamber MFC. Marcus et al. [20] first presented a conduction-based model, which described the biofilm with a dynamic and one-dimensional, multi-species model to simulate the bio-anode. Alavijeh et al. [21] also described a conduction-based model to study complex wastewater treatment and the dynamical electron transfer. The assumptions of electron transfer mechanism used in the above models were often employed in the later studies. Besides, the inhomogeneity of mass transfer of substrate or bacteria was ignored. For example, Pinto et al. [22] governed a time-dependent model by hypothesizing that the charge transfer mechanism from the organics to anode involved a reduced and oxidized intracellular mediators. Sedaqatvand et al. [23] extended the conduction-based model to estimate the design parameters of a MFC treating dairy wastewater. Most of the previous research focused on the conduction mechanism. While researchers found that bacterial electron transfer towards the MFC anode was enabled through self-mediated, such as endogenous mediate pyocyanine and flavin [24,25]. We believe that the study of electrons transfer by an electron shuttle through endogenous extracellular mediators is also very significant. Biofilm forming process on the electrode and the species in the anode compartment are also the key factors affecting current generation of MFC. Xavier et al. introduced a model describing biomass detachment in multidimensional biofilm by using the level set method [26]. This model considered the biofilm structure, activity and the biomass composition to study the biofilm dynamics. Erica et al. [27] theoretically estimated the yield and decay efficient of exoelectrogens in bioelectrochemical systems. Besides, multi-population dynamics models which described various population of biofilm in MEC for hydrogen evolution have been presented to demonstrate that the competition between exoelectrogens and other microorganisms is one of the key factors influencing power output in MECs [28].

The literature review above indicated that most of these models neglected some crucial features in MFCs such as spatial non-uniformities and interior mass transfer characteristics. They assumed that the substrate distribution in anode chamber was uniform and there were no concentration gradients in the biofilm. However, the substrate distribution along the electrode vertical direction is usually non-uniform and it may affect the performance of MFC. Mass transfer process that occurs in this system should be of concern in the scaling-up process. Biofilm is composed of microorganisms and interspace. Owing to the different growing environment, such as different structure of anode materials [29,30] and different shear rate (by controlling different flow rate) of the bulk solution [31,32], the porosity of the biofilm is different. Furthermore, the porosity between exoelectrogens could affect the mass transfer of organic matter and the reduced/oxidized extracellular mediator, which could affect the electron transfer.

External resistance, as a tool to dissipate electrical energy, it can regulate the electrons flow rate and eventually affects the anode potential (E_{an}) and power output. While the E_{an} is the electromotive force that drives electrons to flow, it can affect microbial community structure of biofilm and power output. When E_{an} maintained at a suitable value, high current density and thick biofilm would be achieved [33,34]. Thus, deeply understanding the effect of external resistance on the performance of MFC can provide reference for the design and optimization of the cell.

In this work, a transient, two-dimensional model was developed by coupling the growth of exoelectrogens and methanogens, mass transfer and bio-electrochemical kinetics within the anode chamber in a MFC. This model focused on the dynamic changes of anodic biofilm and mass transfer in both interfacial and bulk solution. The effect of biofilm porosity and external resistance on the electrochemical performance of MFC would be discussed. This model can predict the distribution of the biomass and substrate and provide an intuitive and credible insight on the study of the internal phenomenon in MFC. In this model, the local over-potential was obtained by assuming that the electron transfer from exoelectrogens to the anode was via an electron shuttle through extracellular mediators (such as pyocyanin or microbial phenazine) [24].

To simplify the calculations, the following hypotheses were made: (1) the model focused on electrogenic and methanogenic microbial populations only; (2) exoelectrogens transferred electrons through extracellular mediator; (3) gas transport (e.g. oxygen through cathode and methane through anode) was neglected; (4) acetate was chosen as the sole carbon source in anode chamber; (5) the cathodic oxygen reduction reaction was fixed at a constant over-potential; (6) the pH of bulk liquid was maintained at 7; (7) ionic migration was negligible because of enough supporting electrolyte in the anodic chamber.

2. Materials and methods

2.1. Reactor construction

The single-chamber MFC was constructed with a dual Plexiglass cylindrical chamber reactor as described before [35]. The net volume of this reactor was about 28 mL (4 cm in length and 3 cm in diameter). The anode was hydrophilic carbon cloth (HCN-030, Shanghai Hesen Co., China) without catalyst, while the air cathode was wet-proofed carbon cloth with diffusion layer coated 0.5 mg/cm^2 Pt [36]. The surface area of both anode and cathode is 7.07 cm^2. All experiments were conducted in a constant temperature incubator (GZX-150BS-III, Shanghai CIMO Medical Instrument Manufacturing, China) at 30 °C. Anaerobic granular

sludge supernatant from fruit waste treatment and phosphate buffer solution (PBS, 50 mmol/L) was inoculated for bio-anode acclimation. Until there was a tendency of voltage rising, only PBS solution (50 mmol/L) containing 1.0 g/L acetate was inoculated until the voltage reached 400 mV and kept stable. After that, five more cycles were repeated. For the sake of helping exoelectrogens preferably acclimate to higher current, different external resistances from 1000 Ω to 10 Ω were connected (five downward steps, each resistance operated for 48 h). And five to six cycles were repeated to further enrich exoelectrogens attaching to the anode.

2.2. Analysis

The conductivity of electrolyte was measured by conductivity meter (Lian-Hua Techno., Co., Ltd., China). Polarization test was recorded using DC-voltammetry. The cell voltages (monitored by DAM-3058R data logger, Beijing Art Technology Development Co., Ltd., China) decreased in 23 steps from open circuit voltage (OCV) by decreasing the external resistance from 10,000 to 5 Ω. Before performing polarization curve, MFC was kept under open circuit condition for 30 min and its OCV was measured simultaneously.

3. Mathematical model

This model is based on a two-dimensional batch, transient, single chamber air-cathode MFC [35] with non-limiting cathode reaction rate and the selected calculation area is shown in Fig. 1. It consists of three domains: biofilm, biofilm-electrolyte interface and anodic electrolyte, while the thickness of carbon cloth anode can be neglected, so anode was assumed as a boundary in this model. Since the partial differential equations of mass transfer and electron transfer process are discontinuous, the solution may be singular and this occurs in the interface. Discrete boundary conditions contribute to simplifying this problem in a domain without singular points and can be solved by normal finite element method [37]. Thus each layer was assumed to have discrete boundary in order to simplify the less-defined interfaces in a real MFC anode. And the biofilm thickness is assumed as 0.02 mm [38,39]. As the formation of biofilm, there was an interface between the solid biofilm and the electrolyte, and substrates diffused through this interface to the biofilm. The electron was transported by an electron shuttle through extracellular mediator to the anode. The reactions in the anode chamber include electrochemical reactions on exoelectrogens as (1), (2) and chemical reaction on methanogens as (3):

$$\text{Acetate} + \text{Mox} \xrightarrow{Xe} \text{Mred} + CO_2 \tag{1}$$

$$\text{Mred} \rightarrow \text{Mox} + 2e^- + 2H^+ \tag{2}$$

$$\text{Acetate} \xrightarrow{Methanogens} CH_4 + CO_2 \tag{3}$$

where Mred and Mox are the reduced and oxidized forms of the extracellular mediators, respectively. Xe represents the exoelectrogens.

3.1. Mass conservation equations

The mass transport process focuses on the transport of the substrate and extracellular mediator. The equation for the general mass conservation in anolyte can be written as follows:

$$\frac{\partial c_i}{\partial t} + \nabla\cdot(-D_i\nabla c_i) = R_i \tag{4}$$

$$N_i = -D_i\nabla c_i \tag{5}$$

where c_i stands for the concentration, D_i represents the diffusion coefficient, R_i represents the molar generation rate of species i, N_i represents the mass flux, i represents substrate, extracellular mediator.

While the biofilm could be considered as a porous solid matrix, the porosity of biofilm would affect the mass diffusion to anode. The mass transport controlling equation in biofilm could be written as below:

$$\epsilon_p \frac{\partial c_i}{\partial t} + c_i\frac{\partial_p}{\partial t} + \nabla\cdot N_i = R_i \tag{6}$$

$$N_i = -D_i^{eff}\nabla c_i \tag{7}$$

$$D_i^{eff} = \frac{\epsilon_p}{\tau_{F,i}}D_i \tag{8}$$

where ϵ_p represents the porosity of biofilm, D_i^{eff} is the effective diffusion coefficient of species i, which is related with the porosity, N_i represents the mass flux. And D_i^{eff} is corrected by Bruggeman approximation [40], the correction factor $\tau_{F,i}$ is defined as:

$$\tau_{F,i} = \epsilon_p^{-\frac{1}{2}} \tag{9}$$

For a batch mode MFC, the molar generation rate (R_i) of species substrate, exoelectrogens and methanogens can be defined as equations in Pinto et al. [22], while the molar generation rate of extracellular mediator is related to both the acetate consumption rate by exoelectrogens and the mediator yield. These equations can be written as follow:

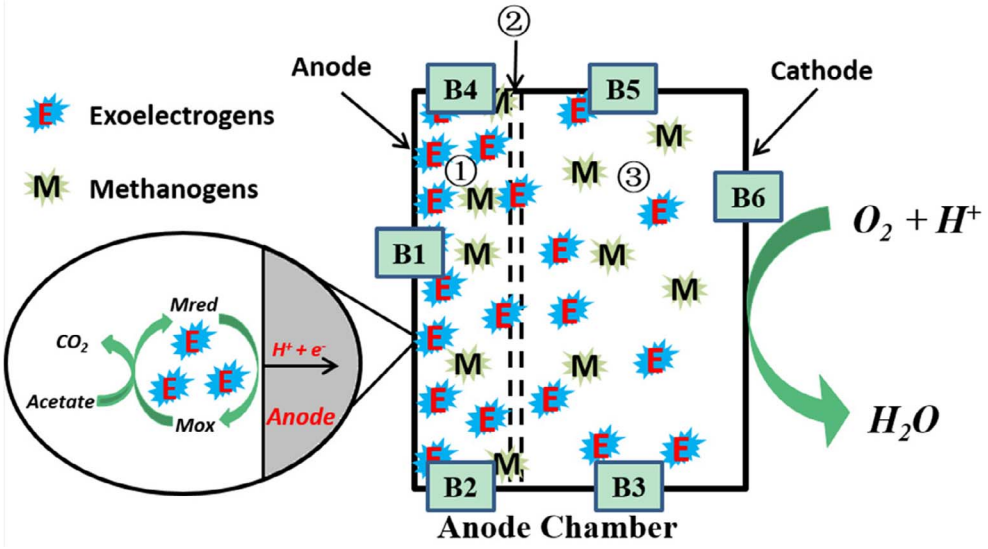

Fig. 1. Schematic of the geometric computational domain of MFC model (① biofilm, ② biofilm-anolyte interface and ③ anolyte, B1–B6 represents boundaries).

$$R_s = -q_e c_{x_e} - q_m c_{x_m} \tag{10}$$

$$R_{x_e} = \mu_e c_{x_e} - K_{d,e} c_{x_e} - \alpha_e c_{x_e} \tag{11}$$

$$R_{x_m} = \mu_m c_{x_m} - K_{d,m} c_{x_m} - \alpha_m c_{x_m} \tag{12}$$

$$R_{Mred} = Y * q_e c_{x_e} \tag{13}$$

$$R_{Mox} = -Y * q_e c_{x_e} \tag{14}$$

where e, m represent exoelectrogens and methanogens, respectively. c_{x_e}, c_{x_m} are the concentration of exoelectrogens and methanogens, respectively. q_e and q_m are the substrate consumption rates by exoelectrogens and methanogens, respectively. μ_e, μ_m represent the growth rates; $K_{d,e}$, $K_{d,m}$ are the decay rate of exoelectrogens and methanogens, and α_e, α_m are the dimensionless biofilm retention constants. Y represents the mediator yield with per molar acetate consumption. Subscript Mred and Mox represent the extracellular mediators.

Biofilm retention in the anode chamber is described by assuming that biomass growth is limited by the maximum attainable biomass concentration. Thus, there is no biofilm washout at bio-anode initial acclimation state until the biofilm reaches its steady state. In the steady state, the net growth rate of biofilm is equal to its decay rate. The balance of anaerobic digestion model NO.1 (ADM1) could be used in this batch mode, two-phase biofilm growth model [41]. Therefore, this biofilm growth can be described with a biomass retention parameter α (s^{-1}) as follows:

$$\alpha_i = \begin{cases} \frac{\mu_e c_{x_e} - K_{d,e} c_{x_e} + \mu_m c_{x_m} - K_{d,m} c_{x_m}}{c_{x_e} + c_{x_m}}, & if\ (c_{x_e} + c_{x_m} > c_{x_{max,i}}) \\ 0, & otherwise \end{cases} \tag{15}$$

where $c_{x_{max,i}}$ is the maximum attainable biomass concentration. To distinguish the existence of the anaerobic microorganism, different $c_{x_{max,i}}$ values were used for exoelectrogens and methanogens with $c_{x_{max,m}} > c_{x_{max,e}}$.

3.2. Kinetic equations

In the growth process of exoelectrogens, the production and consumption of extracellular mediators and substrate exert an effect on the metabolism and electrons transfer. While for the growth of methanogens, the anaerobic digestion is only limited by concentration of substrate. Thus, using multiplicative Monod kinetics and Monod kinetics to describe metabolism rate of exoelectrogens and methanogens, respectively [22], and the rates are determined as follows:

$$\mu_e = \mu_{max,e} \frac{S}{K_{S,e} + S} \frac{c_{Mox}}{K_M + c_{Mox}} \tag{16}$$

$$\mu_m = \mu_{max,m} \frac{S}{K_{S,m} + S} \tag{17}$$

$$q_e = q_{max,e} \frac{S}{K_{S,e} + S} \frac{c_{Mox}}{K_M + c_{Mox}} \tag{18}$$

$$q_m = q_{max,m} \frac{S}{K_{S,m} + S} \tag{19}$$

where $\mu_{max,e}$, $\mu_{max,m}$ are the maximum growth rate of exoelectrogens and methanogens, respectively. $q_{max,e}$, $q_{max,m}$ are the maximum substrate consumption rate of exoelectrogens and methanogens, respectively; and $K_{S,e}$, $K_{S,m}$ and K_M are the half-saturation rate constant of Monod equation of exoelectrogens, methanogens and extracellular mediator, respectively; c_{Mox} is the concentration of oxidized mediator.

3.3. Electrochemical kinetics

To describe the anodic bio-electrochemical reaction kinetics, the Bulter-Volmer equation was used:

$$i_E = i_{0,an} * \left[\frac{c_{Mred}}{c_{ref,Mred}} \exp\left((1-\beta) \frac{F}{RT} \eta_{act} \right) - \frac{c_{Mox}}{c_{ref,Mox}} \exp\left(-\beta \frac{F}{RT} \eta_{act} \right) \right]. \tag{20}$$

$$I_E = i_E * A_{an} \tag{21}$$

where i_E is the bio-electrochemical reaction kinetics-current density ($A \cdot m^{-2}$). $i_{0,an}$ is the exchange current density for extracellular mediator oxidation; β is the transfer coefficient; $c_{ref,Mox}$, $c_{ref,Mred}$ are the concentration of oxidized/reduced extracellular mediator in reference conditions, respectively, which are set as 1 mol m^{-3} [16]. F, R and T are Faraday constant, gas constant and temperature, respectively. η_{act} is the activation over-potential, I_E is the current, and A_{an} is the anode surface area.

The actual voltage of MFC (V_{cell}) is lower than the equilibrium potential owing to the losses of activation, ohmic and concentration. In this anodic bio-electrochemical reaction, the oxidized/reduced extracellular mediator is the electron transfer mediator, therefore, the concentration loss (η_{conc}) is mainly derived from the mediator concentration difference between bulk solution and anode surface. For simplification, the losses of cathode potential was set as a constant value V_C. By summation of all polarization losses, the cell voltage can be written as:

$$V_{cell} = V_C - E_{A,thermo} - (\eta_{act} + \eta_{ohm} + \eta_{conc}) \tag{22}$$

$$\eta_{ohm} = I_E^* R_{int} \tag{23}$$

$$\eta_{conc} = \frac{RT}{2F} \log\left(\frac{c_{Mox} * c_H^2}{c_{Mred}} \right) \tag{24}$$

where $E_{A,thermo}$ is the extracellular mediator thermodynamic equilibrium potential, R_{int} is the internal resistance, and c_H is the concentration of H^+ in atholyte. According to Eqs. (22)-(24), the activation over-potential of anode can be written as:

$$\eta_{act} = V_C - E_{A,thermo} - I_E * (R + R_{int}) - \frac{RT}{2F} \log\left(\frac{c_{Mox}^* c_H^2}{c_{Mred}} \right) \tag{25}$$

3.4. Boundary conditions

Boundary conditions are required to limit the computational region of each control equation. There are four boundaries in this model:

1) For the contact interfaces between the anode electrode and the biofilm (boundary B1 in Fig. 1), where are permeable to electrons, while are impermeable to the acetate, exoelectrogens and methanogens. The interfaces control equation is as follows:

$$\underset{n}{\overrightarrow{\quad}} \cdot \boldsymbol{N_j} = \sum_m R_{j,m} \tag{26}$$

$$R_{j,m} = \frac{\nu_{j,m} i_E}{n_m F} \tag{27}$$

$$\underset{n}{\overrightarrow{\quad}} \cdot N_g = 0 \tag{28}$$

where $\underset{n}{\rightarrow}$ represents the normal direction to electrode; N_j represents the mass flux of mediators; $\nu_{j,m}$ is the stoichiometric coefficient; n_m represents the number of electrons ($n_m = 2$); and m represents the two forms (oxidized/reduced) of extracellular mediator. N_g represents the mass flux of acetate, exoelectrogens and methanogens.

2) The four boundaries B2 to B5 in Fig. 1 are the upper and lower symmetric boundaries and all the variables in the region are treated as the symmetric boundary at these boundaries:

$$\frac{\partial c_s}{\partial y} = 0, \frac{\partial c_{x_e}}{\partial y} = 0, \frac{\partial c_{x_m}}{\partial y} = 0, \frac{\partial \varphi}{\partial y} = 0 \quad (29)$$

3) The boundary located at the interface between the biofilm and the electrolyte, in which only mass transfer occurs:

$$\frac{\partial \varphi}{\partial x} = 0 \quad (30)$$

$$\frac{\partial c_s}{\partial x} = R_i \quad (31)$$

where i represents the acetate, bacteria and extracellular mediators.

4) Boundary B6 in Fig. 1 is the contact interface between cathode and electrolyte, where the cathodic potential was assumed a constant value, and is impermeable to the acetate, bacteria and extracellular mediators. The interfaces control equation is as follows:

$$-\underset{n}{\longrightarrow} \cdot N_i = 0 \quad (32)$$

$$\varphi_c = V_c \quad (33)$$

3.5. Simulation procedure and parameters

Based on the finite element method, the governing partial differential equations were solved in COMSOL Multiphysics and MATLAB, and the operation parameters of MFC and electrochemical parameters are given in Table 1.

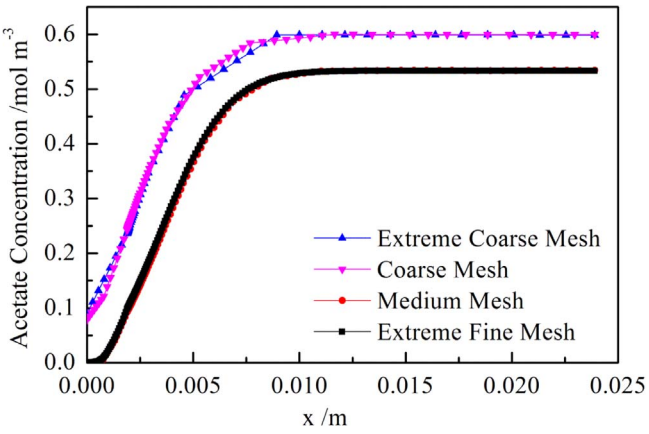

Fig. 2. Grid independent study for acetate concentration along the anode vertical direction using four sets of triangular elements number.

3.6. Grid independence study

This model was meshing with an unstructured triangular grid element. To determine if the predictions are grid-independent, four different total numbers of triangular elements (1538, 2968, 4389, 18,408) of the acetate concentrations along anode vertical direction are presented in Fig. 2. As the grid quality increased, the deviation from model

Table 1
Operation parameters of the MFC, physicochemical properties and bio-electrochemical kinetics parameters used in simulation.

Parameters	Description	Value	Units	Ref.
Structure parameters				
V_{an}	Volume of anode compartment	0.03	L	Experimental condition
A_{an}	Surface area of anode	7.07	cm^2	Experimental condition
L_f	Thickness of biofilm	200	μm	[38,39]
L_b	Thickness of bulk solution	4	cm	Experimental condition
Operation conditions				
$c_{0,Ac}$	Initial concentration, acetate	12.20	$mol\ m^{-3}$	Experimental condition
$c_{0,H}$	Initial concentration, H^+	1×10^{-7}	$mol\ L^{-1}$	Experimental condition
$c_{0,M}$	Initial concentration, extracellular mediator	0	$mol\ L^{-1}$	Experimental condition
T	Temperature	303.15	K	Experimental condition
p^{in}	Anode/Cathode inlet pressure	101,325	pa	Experimental condition
σ_l	Electrolyte conductivity	7.67	$ms\ cm^{-1}$	Experimental condition
Diffusivities				
D_{Ac}	Diffusion coefficient in liquid, acetate	1.21×10^{-9}	$m^2\ s^{-1}$	[43]
D_M	Diffusion coefficient in liquid, extracellular mediator	7.87×10^{-9}	$m^2\ s^{-1}$	Estimated
Biofilm kinetics				
$q_{max,e}$	Maximum substrate consumption rate, exoelectrogens	4.86×10^{-5}	s^{-1}	[28]
$q_{max,m}$	Maximum substrate consumption rate, methanogens	4.90×10^{-5}	s^{-1}	[28]
$\mu_{max,e}$	Maximum growth rate, exoelectrogens	2.31×10^{-5}	s^{-1}	[28]
$\mu_{max,m}$	Maximum growth rate, methanogens	1.16×10^{-6}	s^{-1}	[28]
$K_{S,e}$	Half-saturation rate constant of Monod equation, exoelectrogens	0.244	$mol\ m^{-3}$	[28]
$K_{S,m}$	Half-saturation rate constant of Monod equation, methanogens	0.976	$mol\ m^{-3}$	[28]
K_M	Half-saturation rate constant of Monod equation, intracellular mediator	0.1	$mol\ m^{-3}$	[28]
$K_{d,e}$	Biomass decay rate, exoelectrogens	4.63×10^{-7}	s^{-1}	[28]
$K_{d,m}$	Biomass decay rate, methanogens	2.31×10^{-8}	s^{-1}	[28]
$c_{xmax,e}$	Maximum attainable biomass concentration, exoelectrogens	20.81	$mol\ m^{-3}$	[28]
$c_{xmax,m}$	Maximum attainable biomass concentration, methanogens	21.34	$mol\ m^{-3}$	[21]
Y	Mediator yield when consuming per molar acetate	3.03	–	[43]
Bio-electrochemical reaction kinetics parameters				
$i_{0,an}$	Exchange current	0.04	$A\ m^{-2}$	[42]
β	Transfer coefficient	0.489	–	[42]
$E_{an,thermo}$	Intracellular mediator thermodynamic equilibrium potential	0.429	V	Measured
R_{int}	Internal resistance	200	Ω	Experimental condition
V_C	Cathode potential	0.68	V	Experimental condition

prediction reduced gradually, and the grid quality decreased with a decrease in the grid numbers when using unstructured grid [44]. As shown in Fig. 2, with the grid numbers decreased, especially with the extreme coarse mesh, the acetate concentration deviation increased to 4%, while with medium mesh, the deviation was lower than 0.4%. However, the numerical solution using the extreme fine mesh would reduce the computational efficiency. Hence, numerical modeling with a grid numbers of 4389 (medium mesh) is sufficient for this simulations.

4. Results and discussion

4.1. Model validation

In this batch mode MFC model, three-dimensional (3D) model of MFC was developed firstly to discuss the impact of biofilm porosity and external resistance on mass distribution and electricity generation performance. As shown in Fig. S1, the simulation results from 3D model indicated that the acetate concentration in the MFC reactor distributes uniformly over the zy plane (Fig. S1b), while distributes inhomogeneous over the xy plane (Fig. S1a). Thus, two-dimensional (2D) model was developed in this work to discuss the internal mass transfer and this 2D model saved the computing resources as well.

To verify this model, the cell performance simulated by this model was compared with experimental data under the same operation conditions as shown in Fig. 3. It can be found that the MFC polarization curve that resulted from the numerical predictions and the MFC polarization curve that obtained from experimental data were generally in good agreement (Fig. 3a). The deviation between the simulation data and the experimental data might be due to the ignored factors in building the model (details in model assumption). Besides, the variation trend of the current that predicted in the numerical simulation as the reaction proceeding closely followed experimental measured current at same operation condition. The larger discrepancies were observed around day 1–2 and day 5, which were attributed to a non-zero current (infinitesimal) at the beginning (t = 0) assumed in the model to make model convergent.

4.2. Effect of biofilm porosity

A typical cylindrical single-chamber MFC was used to study the effect of biofilm porosity on the behavior of MFC. In fuel cells with porous electrode or catalyst layer on the electrode, the porosity could affect mass transfer. With higher porosity, the mass transfer would be much easier, and the transfer resistance would decrease [45,46]. Chemical reaction, bioelectrochemical reaction and mass transfer existed in the biofilm, which was considered as a porous solid matrix in this model. Different growing environment of anode biofilm would affect the porosity of biofilm as described above [29,31], and the porosity would affect the mass transfer [46] and current generation ability in MFC. According to the previous work, the biofilm porosities were set from 0.5 to 0.9 in this model [47,48]. Fig. 4 shows the influence of biofilm porosities on current generation and the extracellular mediator distribution at start-up phase (0.8 d) and steady phase (10.8 d), respectively. As shown in Fig. 4, the extracellular mediator distribution and MFC performance were much different in the start-up phase and steady phase while the difference among various porosities was small.

In the start-up phase, an increase in biofilm porosity led to an increase in Mox concentration, while the Mred concentration change was complex. The Mred concentration was positively correlated with the porosity in the region between anode and biofilm-electrolyte interface, but negatively correlated with the porosity in bulk solution as predicted by this model (Fig. 4a). This phenomenon is owing to the effects of chemical reactions, bioelectrochemical reactions and the mass transfer resistance under different biofilm porosities. Fig. 4b indicated that the current platform of this system rose as porosity increased, while the effect diminished as the biofilm porosity being higher than 0.7. This result declared that higher porosity could promote electron transfer to anode and eventually facilitated the bioelectrochemical reaction rate. At the region near anode, although the higher porosity would result in lower Mred mass transfer resistance and higher electron transfer rate, it would speed up the reaction rate of reaction 1 and eventually result in higher Mred concentration. In bulk solution, only reaction 1 and mass transfer happened as for exoelectrogens. Although the Mred generated by suspended exoelectrogens in bulk solution didn't contribute to current generation directly, since it could not effectively diffuse due to the higher mass transfer resistance at lower porosities, which led to Mred concentration increased as porosity decreased in bulk solution. With these reactions proceeding, the biofilm became thicker and more exoelectrogens could transfer electrons to the anode, which accelerated the electron transfer from Mred to Mox. And higher biofilm porosity was conducive to reduce the mass transfer resistance. Eventually, the coupling effect of mass transfer and bioelectrochemical reaction promoted the electron transfer from anode to the external circuit at higher porosities.

In the steady phase, Mred concentration increased as porosity increased along the anode vertical direction (Fig. 4c). There were enough exoelectrogens in the biofilm for conversion of Mox and Mred, the concentration of Mox and Mred were not the cell performance determining factor, and the biofilm porosities nearly had no impact on current generation (Fig. 4d). Similarly, though the current platforms at different porosities were similar, mass transfer resistance increased with lower porosity while reaction rate decreased (Reaction (1), (2)). These three processes' interaction made the Mred concentration positively correlated with the biofilm porosity (Fig. 4c). The steady current

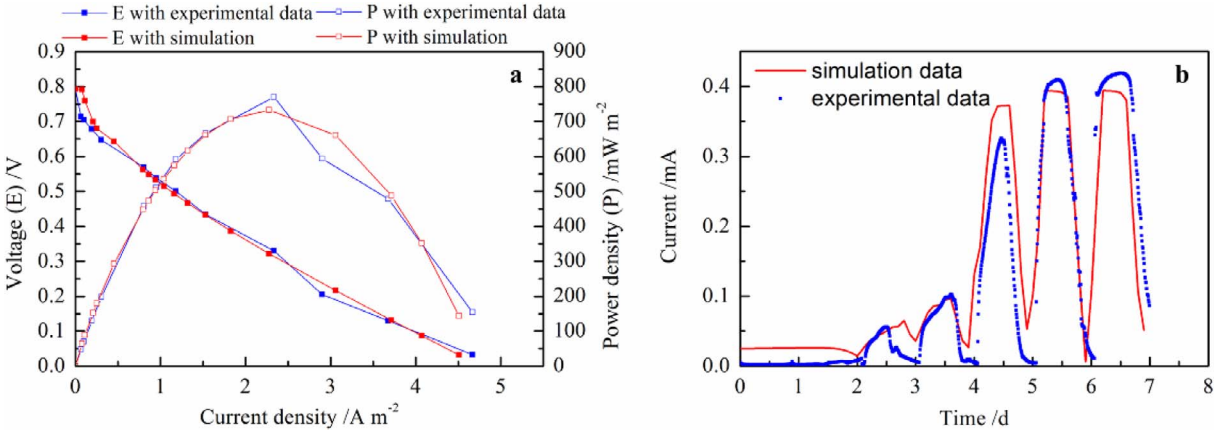

Fig. 3. Comparison of MFC performance predicted by models and experimental data: a) polarization curve and b) current generation.

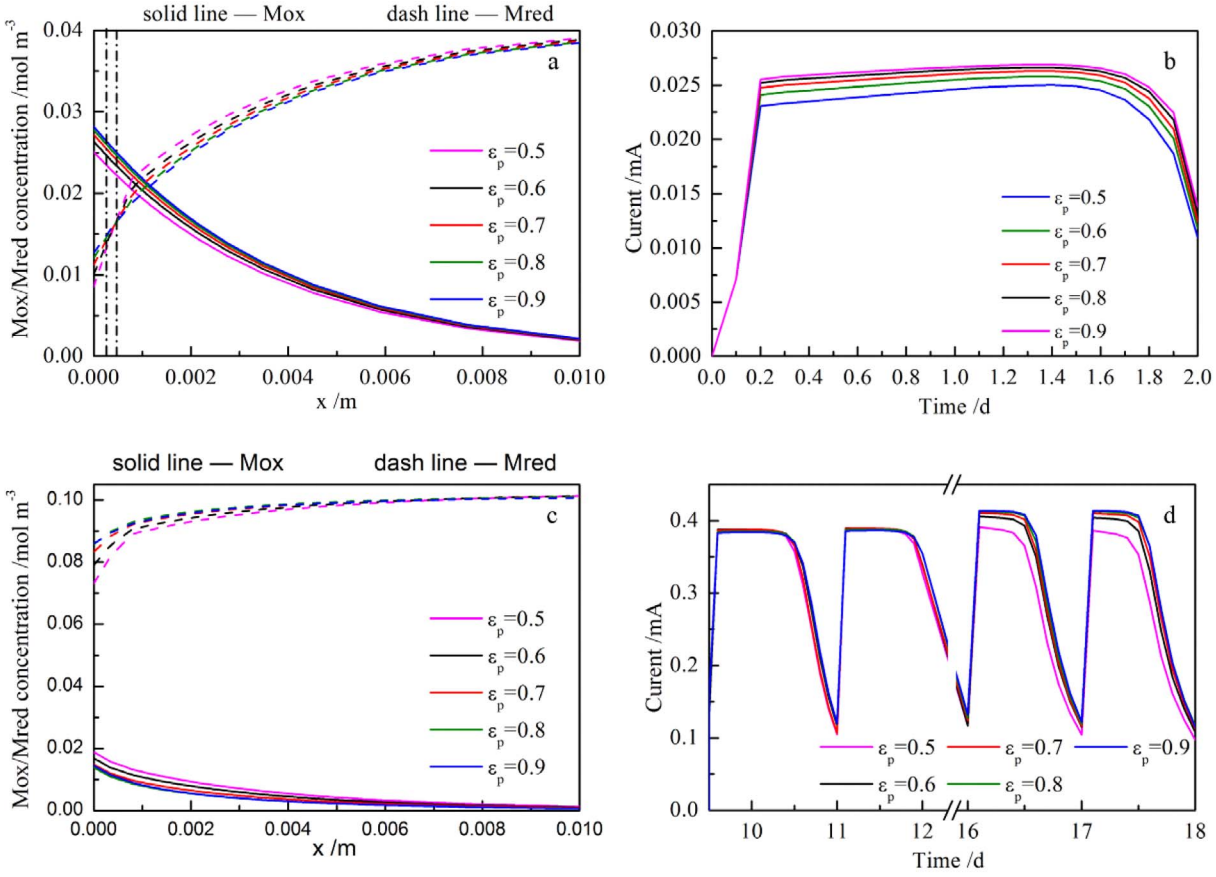

Fig. 4. Simulation results for different biofilm porosity: a) extracellular mediator concentration along the anode vertical direction at 0.8 d; b) MFC performance at start-up phase; c) extracellular mediator concentration along the anode vertical direction at 10.8 d; d) MFC performance at steady phase (black dash vertical line in (a) represents biofilm-bulk solution interface).

of this system is consistent with different biofilm porosities in the beginning 16 days as exhibited in Fig. 4d. As MFC proceeded more than 16 d, the decay of exoelectrogens was more prominent than the accumulation (data shown in Fig. S2), and the reaction rate of Mred to Mox limited the electrons transfer to anode. And higher porosities were beneficial to current generation (Fig. 4d).

Five MFCs with varying biofilm porosity were simulated using the proposed model to discuss the effect on exoelectrogens concentration as shown in Fig. 5. As displayed, there were obvious differences in the exoelectrogens concentration as a result of the biofilm porosity and the system with biofilm porosity of 0.9 had the highest exoelectrogens concentration. In the middle section of biofilm as shown in Fig. 5f, the exoelectrogens concentration increased as biofilm porosities increased in the biofilm domain. Besides, the exoelectrogens concentration gradient decreased as the biofilm porosities increased in the biofilm domain, which indicated that the higher of the biofilm porosities, the more homogeneous of the exoelectrogens concentration distribution was in the biofilm. While near the bulk solution (interface between biofilm and bulk solution), the differences among various biofilm porosities were small and the exoelectrogens concentration in the biofilm-electrolyte interface was lower than that in biofilm except with biofilm porosities of 0.5, which indicated that higher biofilm porosities was beneficial to exoelectrogens colony in biofilm.

When considering the extracellular mediators' concentration at different biofilm porosities. We found that MFC with biofilm porosity of 0.9 had the highest Mred concentration but the lowest Mox concentration, and there were obvious differences in the concentration of Mox and Mred with different biofilm porosities (Fig. S3). It indicated that higher biofilm porosity was helpful to exoelectrogens growth and the bioelectrochemical reaction rate, which led to the accumulation of Mred. However, the Mred concentration near the electrode surface was usually lower than that in bulk solution. This was because that the bioelectrochemical reaction (Reaction (2)) mainly happened within the biofilm and biofilm electrolyte interface region. When the biofilm porosity was higher, the transfer of Mox/Mred to the electrode was faster, and electrons transfer to anode was accelerated, too.

Methanogens could only convert acetate to methane and carbon dioxide without electrons transfer to anode. They could compete with the exoelectrogens for consuming acetate undesirably and led to electrons loss on the anode. It is expected that there would be a significant decrease in electrons loss if methanogens growth could be inhibited [49–51]. The distribution of methanogens at various porosities was simulated after operating 18 d in Fig. 6. As shown in Fig. 6, the higher biofilm porosity limited the growth of methanogens, which was opposite to the effect on exoelectrogens. Fig. 6f shows the methanogens concentration in the middle section of biofilm along the anode vertical direction, which further explained that higher biofilm porosities restrained the methanogens growth in biofilm and more exoelectrogens could contribute to transferring electron from acetate to anode. Fig. 7 revealed that the higher biofilm porosity was beneficial to acetate transfer through biofilm. At the end of each batch cycle, the acetate's concentration is nearly consumed at the anode boundary with different biofilm porosities. The acetate concentration gradient decreased with the increase of biofilm porosities except with porosity of 0.7, and that with biofilm porosity of 0.8 and 0.9 had similar acetate concentration gradient at the whole computing domain. This is because with higher biofilm porosity, more acetate transfer to biofilm for bacteria consuming for electron transfer (Reaction (1), (2)), which is beneficial for current generation. And this also led to low acetate concentration in bulk solution. Thus, with the combining effect of bio-electrochemical

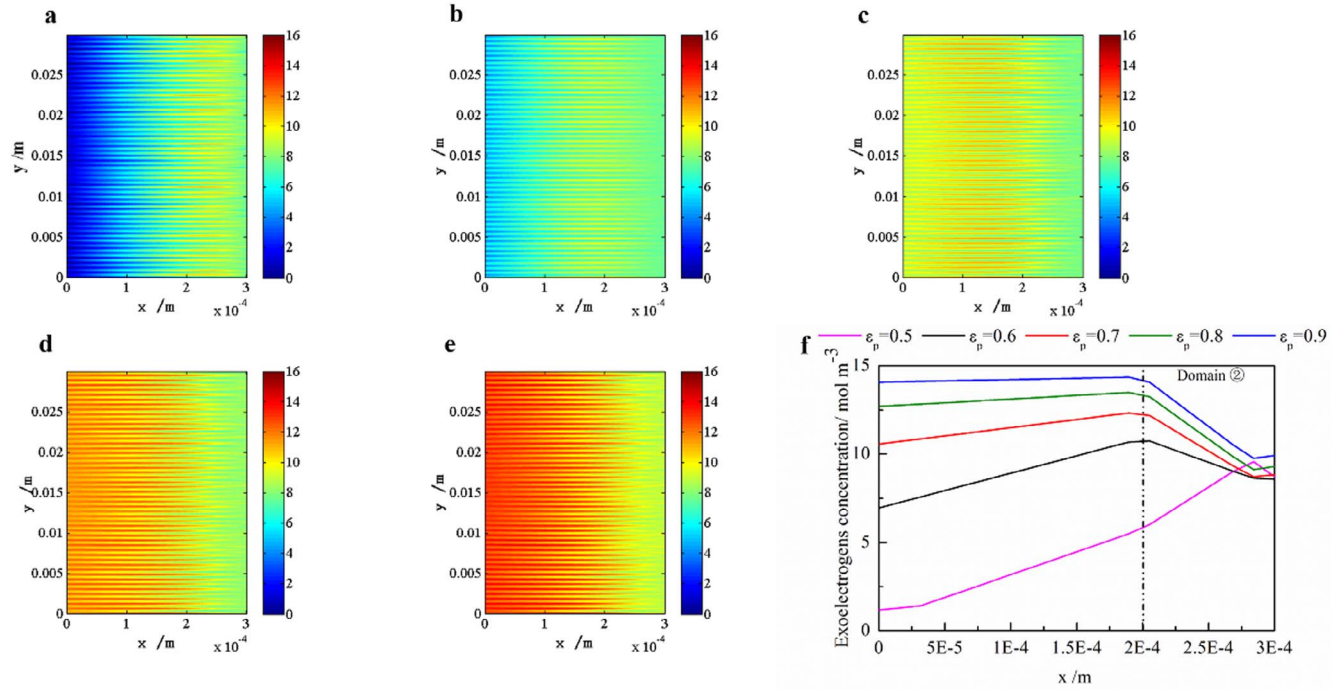

Fig. 5. Exoelectrogens distribution in biofilm at different porosities of: a) 0.5, b) 0.6, c) 0.7, d) 0.8, e) 0.9 and f) Exoelectrogens concentration in the middle section of biofilm along the anode vertical direction at 18 d.

reaction and mass transfer resistance, the acetate concentration gradient was the lowest and higher current generation was obtained with biofilm porosity of 0.9 in this model. Although higher porosity is responsible for mass transfer, acetate concentration in bulk solution with biofilm porosity of 0.7 was higher than that with the biofilm porosity of 0.6. This might be caused by the lower density of bacteria in the biofilm, which lower the rate of acetate consumption in the biofilm (Figs. 5 and 6). The higher acetate concentration gradient with biofilm porosity of 0.5 is resulted from the higher mass transfer resistance at lower biofilm porosities. The above results declared that higher biofilm porosity strengthened both the substrate distribution and the competitiveness of exoelectrogens to degrade acetate. Meanwhile, higher porosity inhibited methanogenesis and reduced methanogenic electrons loss.

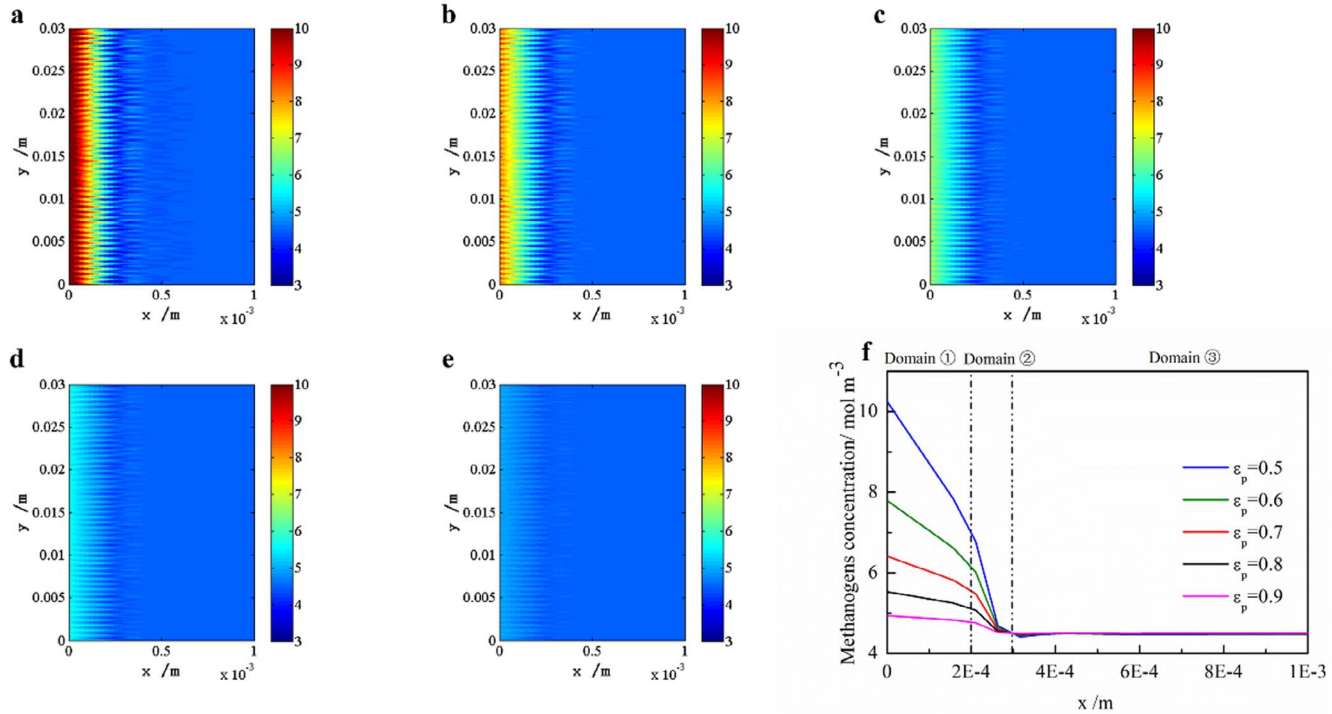

Fig. 6. Methanogens distribution at different biofilm porosities of: a) 0.5, b) 0.6, c) 0.7, d) 0.8, e) 0.9 and f) Methanogens concentration in the middle section of biofilm along the anode vertical direction at 18 d.

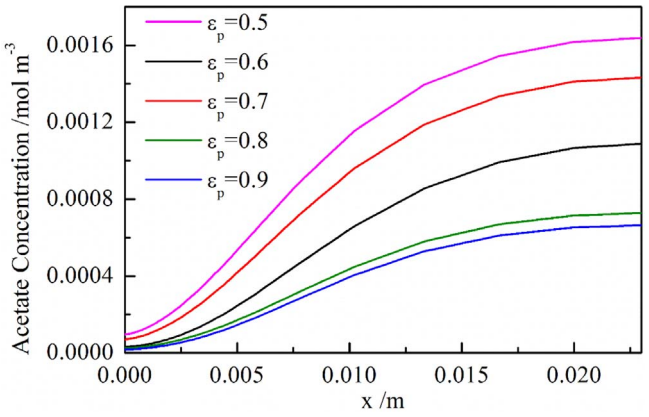

Fig. 7. Acetate concentration along the anode vertical direction with different biofilm porosity at 18 d.

4.3. Effect of external resistance

Optimizing the growth conditions for exoelectrogens is an important consideration to improve the MFC performance, especially shortening start-time. Optimizing external resistance is actually beneficial to the anode biofilm formation and power output [52,53]. Fig. 8 depicts the exoelectrogens and methanogens distribution at external resistances of 20, 200, 470 and 1000 Ω after 10 d operation. As shown in Fig. 8, the exoelectrogens concentration decreased slightly when the MFC was operated with higher external resistance after 10 d, while the methanogens concentration just changed in the opposite trend. That was, the microbial community in biofilm was influenced by external resistance. Exoelectrogens were more dominant on the anode with lower external resistance compared with methanogens. The electricity production is dependent on the final electrons transfer step, i.e., from bacteria to anode [1]. The higher exoelectrogens concentration contributed to transferring more electrons to the anode. While the higher external resistance restricted the current and this may not help exoelectrogens to colonize the anode. The methanogens had diverse distribution near biofilm, where suffered fierce competition of substrate consumption with exoelectrogens. With lower external resistance applied, the exoelectrogens became more competitive compared with methanogens.

As displayed in Fig. 9a, with the same external resistance, acetate concentration increased with the increase of the distance from the anode. Besides, external resistance had significant impact on the microbial communities (Fig. 8). The exoelectrogens and methanogens distribution at various resistances was different, thus higher external resistance resulted in higher acetate concentration at the same distance from the anode. The reaction rate of exoelectrogens consuming acetate is definitely related to the final electron transfer step, which could be explained by the Mox and Mred transfer. Fig. 9b showed the Mox and Mred distribution along the anode vertical direction. It was apparent that the external resistance limited the electron transfer rate, because the Mox concentration decreased with the increase of external resistance at the same position, while Mred concentration basically increased. That was, external resistance had opposite effect on the electrons transfer from Mred to Mox.

It is worth to mention that the step determining the electron transfer from anode to external circuit is associated with the exoelectrogens colonization on the anode. The external resistance affected the anode potential, and finally affected the bacteria colonization. In this work,

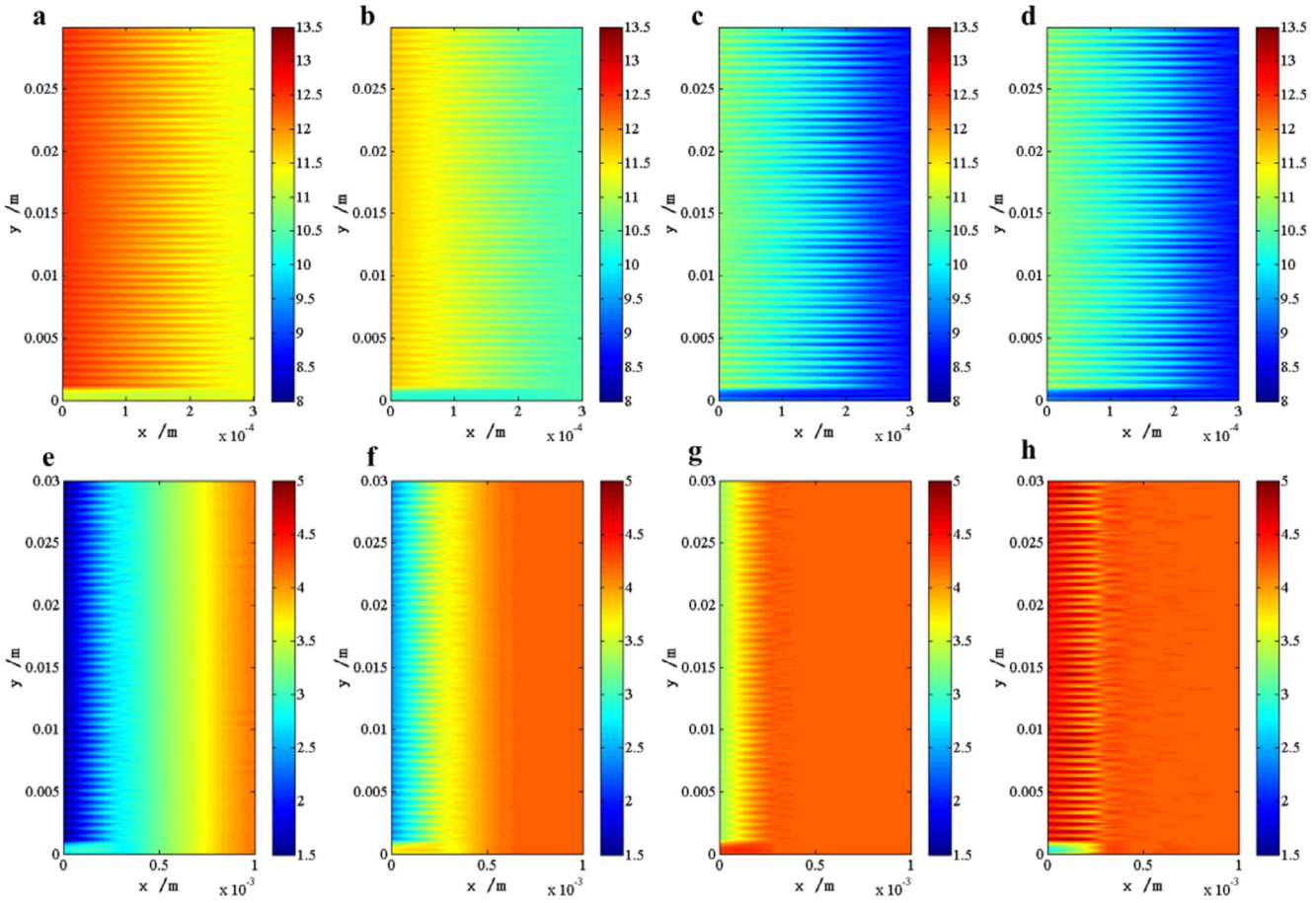

Fig. 8. Concentration of exoelectrogens (a-d) and methanogens (e-h) after 10 d at different external resistances: a) and e) 10 Ω, b) and f) 200 Ω, c) and g) 470 Ω, d) and h) 1000 Ω.

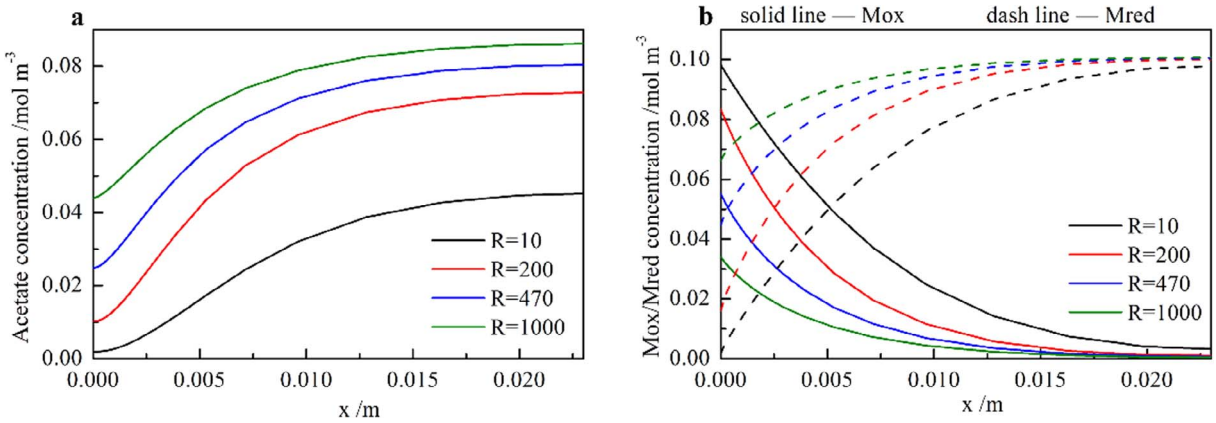

Fig. 9. Mox/Mred (a) and acetate (b) distribution along anode vertical direction at different external resistance.

the simulation result revealed that anode over-potential diminished with the increase of external resistance (Fig. S4). Higher over-potential is responsible for anode polarization, which could accelerate electrochemical reaction rate [54]. Besides, researchers have testified that bacteria with higher electron transfer activity prefer colonizing the anode with low external resistance [55,56], which is in agreement with our simulation results (Fig. 8). Previous research revealed that bacterial communities varied according to the anode potential [57]. And controlling the external resistance can directly affect the anode potential by controlling anode over-potential (Fig. S4), which is more feasible than setting anode potential, and in turn, it can affect the distribution of exoelectrogens and methanogens. External resistance provides a tool to select the electrochemically active microbial communities and produces extracellular mediators as electron shuttles to improve MFCs performance. The results from this model indicated that investigation of the distribution and transfer processes of microbial communities, Mox/Mred and substrate in MFCs provided a more reliable designing method for MFCs operation, which may further provide guidance for the optimization of MFCs.

5. Conclusion

In this study, we have developed a model to discuss the microorganism growth, mass transfer and bio-electrochemical kinetics within the anode chamber in MFC. The model was founded by a finite element method. The simulation results revealed that the biofilm porosity directly affected the microbial community distribution and electrochemical performance in MFC. At start-up phase, higher biofilm porosity was beneficial to electricity generation; while at steady phase, biofilm porosity nearly had no effect on electricity generation in the beginning 16 d, and the current generation was positively correlated with biofilm porosity after 16 d. Besides, when the biofilm porosity increased, the exoelectrogens concentration increased, which was opposite to methanogens. By investigating the effect of external resistance, the results indicated that lower external resistance was beneficial for exoelectrogens growth and colonization. MFC with lower external resistance not only tended to form biofilm with more exoelectrogens, but also produced a higher extracellular mediator concentration.

Obviously, compared with the previous models, this model assumed non-uniform mass transfer and could predict the substrate diffusion more accurately. Understanding the mass transfer of each substrate, the effect of biofilm porosity and external resistance by discussing the interactions between bacteria and substrate can help to explain the phenomenon observed and improve theoretical knowledge of MFC and to optimize the design and operation parameters. For example, it can be used to control the biofilm porosity by adjusting different flow rate or using different anode materials. It can also be used to improve the electricity generation and exoelectrogens colonization by using suitable external resistance. In brief, understanding the interior process and heterogeneous substrate distribution in MFCs by modeling is especially useful for MFC development.

Acknowledgements

This work is financially supported by National Natural Science Foundation of China for Distinguished Young Scientists (No. 51425603), Science and Technology Planning Project of Guangdong Province, China (No. 2017A020216019) and Natural Science Basic Research Plan in Shaanxi Province of China (Program No. 2017JM5004). W.F. Cai thanks the support from China Scholarship Council (No. 201706280278).

Appendix A. Supplementary data

Supplementary data associated with this article can be found, in the online version, at http://dx.doi.org/10.1016/j.cej.2017.09.189.

References

[1] B.E. Logan, B. Hamelers, R. Rozendal, U. Schröder, J. Keller, S. Freguia, P. Aelterman, W. Verstraete, K. Rabaey, Microbial fuel cells: methodology and technology, Environ. Sci. Technol. 40 (2006) 5181–5192.
[2] A.N. Ghadge, D.A. Jadhav, H. Pradhan, M.M. Ghangrekar, Enhancing waste activated sludge digestion and power production using hypochlorite as catholyte in clayware microbial fuel cell, Bioresource Technol. 182 (2015) 225–231.
[3] G. Zhang, Q. Zhao, Y. Jiao, D. Lee, Long-term operation of manure-microbial fuel cell, Bioresource Technol. 180 (2015) 365–369.
[4] Y. Yang, Z. Lu, X. Lin, C. Xia, G. Sun, Y. Lian, M. Xu, Enhancing the bioremediation by harvesting electricity from the heavily contaminated sediments, Bioresource Technol. 179 (2015) 615–618.
[5] C. Xia, M. Xu, J. Liu, J. Guo, Y. Yang, Sediment microbial fuel cell prefers to degrade organic chemicals with higher polarity, Bioresource Technol. 190 (2015) 420–423.
[6] W. Thung, S. Ong, L. Ho, Y. Wong, F. Ridwan, Y. Oon, Y. Oon, H.K. Lehl, A highly efficient single chambered up-flow membrane-less microbial fuel cell for treatment of azo dye Acid Orange 7-containing wastewater, Bioresource Technol. 197 (2015) 284–288.
[7] C. Sakdaronnarong, A. Ittitanakam, W. Tanubumrungsuk, S. Chaithong, S. Thanosawan, N. Sinbuathong, C. Jeraputra, Potential of lignin as a mediator in combined systems for biomethane and electricity production from ethanol stillage wastewater, Renewable Energy 76 (2015) 242–248.
[8] Y. Park, S. Park, V.K. Nguyen, J. Yu, C.I. Torres, B.E. Rittmann, T. Lee, Complete nitrogen removal by simultaneous nitrification and denitrification in flat-panel air-cathode microbial fuel cells treating domestic wastewater, Chem. Eng. J. 316 (2017) 673–679.
[9] S. Cheng, B. Wang, Y. Wang, Increasing efficiencies of microbial fuel cells for collaborative treatment of copper and organic wastewater by designing reactor and selecting operating parameters, Bioresource Technol. 147 (2013) 332–337.
[10] S. Gupta, A. Yadav, N. Verma, Simultaneous Cr(VI) reduction and bioelectricity generation using microbial fuel cell based on alumina-nickel nanoparticles-dispersed carbon nanofiber electrode, Chem. Eng. J. 307 (2017) 729–738.
[11] X. Chen, H. Sun, P. Liang, X. Zhang, X. Huang, Optimization of membrane stack configuration in enlarged microbial desalination cells for efficient water desalination, J. Power Sources 324 (2016) 79–85.

[12] A.D. Angelo, A. Galia, O. Scialdone, Cathodic abatement of Cr(VI) in water by microbial reverse-electrodialysis cells, J. Electroanal. Chem. 748 (2015) 40–46.
[13] Y. Song, S. Hidayat, H. Kim, J. Park, Hydrogen production in microbial reverse-electrodialysis electrolysis cells using a substrate without buffer solution, Bioresource Technol. 210 (2016) 56–60.
[14] V.M. Ortiz-Martínez, M.J. Salar-García, A.P. de Los Ríos, F.J. Hernández-Fernández, J.A. Egea, L.J. Lozano, Developments in microbial fuel cell modeling, Chem. Eng. J. 271 (2015) 50–60.
[15] C.I. Torres, A.K. Marcus, H. Lee, P. Parameswaran, R. Krajmalnik-Brown, B.E. Rittmann, A kinetic perspective on extracellular electron transfer by anode-respiring bacteria, FEMS Microbiol. Rev. 34 (2010) 3–17.
[16] C. Picioreanu, I.M. Head, K.P. Katuri, M.C.M. van Loosdrecht, K. Scott, A computational model for biofilm-based microbial fuel cells, Water Res. 41 (2007) 2921–2940.
[17] C. Picioreanu, M.C.M. van Loosdrecht, K.P. Katuri, K. Scott, I.M. Head, Mathematical model for microbial fuel cells with anodic biofilms and anaerobic digestion, Water Sci. Technol. 57 (2008) 965–971.
[18] C. Picioreanu, M.C.M. van Loosdrecht, T.P. Curtis, K. Scott, Model based evaluation of the effect of pH and electrode geometry on microbial fuel cell performance, Bioelectrochemistry 78 (2010) 8–24.
[19] Y. Zeng, Y.F. Choo, B. Kim, P. Wu, Modelling and simulation of two-chamber microbial fuel cell, J. Power Sources 195 (2010) 79–89.
[20] A.K. Marcus, C.I. Torres, B.E. Rittmann, Conduction-based modeling of the biofilm anode of a microbial fuel cell, Biotechnol. Bioeng. 98 (2007) 1171–1182.
[21] M.K. Alavijeh, M.M. Mardanpour, S. Yaghmaei, A generalized model for complex wastewater treatment with simultaneous bioenergy production using the microbial electrochemical cell, Electrochim. Acta 167 (2015) 84–96.
[22] R.P. Pinto, B. Srinivasan, M.F. Manuel, B. Tartakovsky, A two-population bio-electrochemical model of a microbial fuel cell, Bioresource Technol. 101 (2010) 5256–5265.
[23] R. Sedaqatvand, M. Nasr Esfahany, T. Behzad, M. Mohseni, M.M. Mardanpour, Parameter estimation and characterization of a single-chamber microbial fuel cell for dairy wastewater treatment, Bioresource Technol. 146 (2013) 247–253.
[24] K. Rabaey, N. Boon, M. Höfte, W. Verstraete, Microbial phenazine production enhances electron transfer in biofuel cells, Environ. Sci. Technol. 39 (2005) 3401–3408.
[25] E. Marsili, D.B. Baron, I.D. Shikhare, D. Coursolle, J.A. Gralnick, D.R. Bond, Shewanella secretes flavins that mediate extracellular electron transfer, Proc Natl Acad Sci U.S.A. 105 (2008) 3968–3973.
[26] J.D.B. Xavier, C. Picioreanu, M.C.M. van Loosdrecht, A general description of detachment for multidimensional modelling of biofilms, Biotechnol. Bioeng. 91 (2005) 651–669.
[27] E.L. Wilson, Y. Kim, The yield and decay coefficients of exoelectrogenic bacteria in bioelectrochemical systems, Water Res. 94 (2016) 233–239.
[28] R.P. Pinto, B. Srinivasan, A. Escapa, B. Tartakovsky, Multi-population model of a microbial electrolysis cell, Environ. Sci. Technol. 45 (2011) 5039–5046.
[29] A. Baudler, M. Langner, C. Rohr, A. Greiner, U. Schroeder, Metal-polymer hybrid architectures as novel anode platform for microbial electrochemical technologies, ChemSusChem 10 (2017) 253–257.
[30] C. Santoro, M. Guilizzoni, J.P. Correa Baena, U. Pasaogullari, A. Casalegno, B. Li, S. Babanova, K. Artyushkova, P. Atanassov, The effects of carbon electrode surface properties on bacteria attachment and start up time of microbial fuel cells, Carbon 67 (2014) 128–139.
[31] W.K. Kwok, C. Picioreanu, S.L. Ong, M. van Loosdrecht, W.J. Ng, J.J. Heijnen, Influence of biomass production and detachment forces on biofilm structures in a biofilm airlift suspension reactor, Biotechnol. Bioeng. 58 (1998) 400–407.
[32] J.H. Tay, Q.S. Liu, Y. Liu, The effects of shear force on the formation, structure and metabolism of aerobic granules, Appl. Microbiol. Biotechnol. 57 (2001) 227–233.
[33] S. Jung, J.M. Regan, Influence of external resistance on electrogenesis, methanogenesis, and anode prokaryotic communities in microbial fuel cells, Appl. Environ. Microbiol. 77 (2011) 564–571.
[34] D.Y. Lyon, F. Buret, T.M. Vogel, J. Monier, Is resistance futile? Changing external resistance does not improve microbial fuel cell performance, Bioelectrochemistry 78 (2010) 2–7.
[35] H. Liu, B.E. Logan, Electricity generation using an air-cathode single chamber microbial fuel cell in the presence and absence of a proton exchange membrane, Environ. Sci. Technol. 38 (2004) 4040–4046.
[36] M. Joshua, C. Shaoan, L. Wenzong, How to make cathodes with a diffusion layer for single-chamber microbial, Fuel Cells (2006).
[37] X.N. Wu, H.D. Han, Discrete boundary conditions for problems with interface, Comput. Methods Appl. Math. 190 (2001) 4987–4998.
[38] D. Sun, S. Cheng, A. Wang, F. Li, B.E. Logan, K. Cen, Temporal-spatial changes in viabilities and electrochemical properties of anode biofilms, Environ. Sci. Technol. 49 (2015) 5227–5235.
[39] D. Sun, J. Chen, H. Huang, W. Liu, Y. Ye, S. Cheng, The effect of biofilm thickness on electrochemical activity of Geobacter sulfurreducens, Int. J. Hydrogen Energy 41 (2016) 16523–16528.
[40] D.A.G. Bruggeman, Berechnung verschiedener physikalischer Konstanten von heterogenen Substanzen. I. Dielektrizitätskonstanten und Leitfähigkeiten der Mischkörper aus isotropen Substanzen, Ann. Phys. Berlin 416 (1935) 636–664.
[41] B. Tartakovsky, S.J. Mu, Y. Zeng, S.J. Lou, S.R. Guiot, P. Wu, Anaerobic digestion model no. 1-based distributed parameter model of an anaerobic reactor: II. Model validation, Bioresource Technol. 99 (2008) 3676–3684.
[42] H.V.M. Hamelers, A. ter Heijne, N. Stein, R.A. Rozendal, C.J.N. Buisman, Butler–Volmer–Monod model for describing bio-anode polarization curves, Bioresource Technol. 102 (2011) 381–387.
[43] S. Ou, Y. Zhao, D.S. Aaron, J.M. Regan, M.M. Mench, Modeling and validation of single-chamber microbial fuel cell cathode biofilm growth and response to oxidant gas composition, J. Power Sources 328 (2016) 385–396.
[44] J.H. Ferziger, M. Peric, Computational Methods for Fluid Dynamics, Springer Science & Business Media, 2012.
[45] L. Li, K. Zheng, M. Ni, M.K.H. Leung, J. Xuan, Partial modification of flow-through porous electrodes in microfluidic fuel cell, Energy 88 (2015) 563–571.
[46] K.S. Salloum, J.R. Hayes, C.A. Friesen, J.D. Posner, Sequential flow membraneless microfluidic fuel cell with porous electrodes, J. Power Sources 180 (2008) 243–252.
[47] D. Frattini, G. Accardo, C. Ferone, R. Cioffi, Fabrication and characterization of graphite-cement composites for microbial fuel cells applications, Mater. Res. Bull. 88 (2017) 188–199.
[48] D. Massazza, R. Parra, J.P. Busalmen, H.E. Romeo, New ceramic electrodes allow reaching the target current density in bioelectrochemical systems, Energy Environ. Sci. 8 (2015) 2707–2712.
[49] K. Chae, M. Choi, K. Kim, F.F. Ajayi, W. Park, C. Kim, I.S. Kim, Methanogenesis control by employing various environmental stress conditions in two-chambered microbial fuel cells, Bioresource Technol. 101 (2010) 5350–5357.
[50] K. Chae, M. Choi, K. Kim, F.F. Ajayi, I. Chang, I.S. Kim, Selective inhibition of methanogens for the improvement of biohydrogen production in microbial electrolysis cells, Int. J. Hydrogen Energy 35 (2010) 13379–13386.
[51] R.C. Tice, Y. Kim, Methanogenesis control by electrolytic oxygen production in microbial electrolysis cells, Int. J. Hydrogen Energy 39 (2014) 3079–3086.
[52] L. Zhang, X. Zhu, J. Li, Q. Liao, D. Ye, Biofilm formation and electricity generation of a microbial fuel cell started up under different external resistances, J. Power Sources 196 (2011) 6029–6035.
[53] H. Rismani-Yazdi, A.D. Christy, S.M. Carver, Z. Yu, B.A. Dehority, O.H. Tuovinen, Effect of external resistance on bacterial diversity and metabolism in cellulose-fed microbial fuel cells, Bioresource Technol. 102 (2011) 278–283.
[54] A.J. Bard, L.R. Faulkner, Electrochemical Methods: Fundamentals and Application, second ed., Wiley, New York, 2001.
[55] K. Rabaey, N. Boon, S.D. Siciliano, M. Verhaege, W. Verstraete, Biofuel cells select for microbial consortia that self-mediate electron transfer, Appl. Environ. Microbiol. 70 (2004) 5373–5382.
[56] S. Srikanth, S. Venkata Mohan, P.N. Sarma, Positive anodic poised potential regulates microbial fuel cell performance with the function of open and closed circuitry, Bioresource Technol. 101 (2010) 5337–5344.
[57] P. Aelterman, S. Freguia, J. Keller, W. Verstraete, K. Rabaey, The anode potential regulates bacterial activity in microbial fuel cells, Appl. Microbiol. Biotechnol. 78 (2008) 409–418.